06 Apr 1995, 10:30 am - 12:30 pm

Effective Stress Liquefaction Analysis at the Wildlife Site

P. M. Byrne
University of British Columbia, Canada

J. McIntyre
Klohn-Crippen Consultants Ltd., Canada

Proceedings: Third International Conference on Recent Advances in Geotechnical Earthquake Engineering and Soil Dynamics, April 2-7, 1995, Volume I, St. Louis, Missouri

Effective Stress Liquefaction Analysis at the Wildlife Site

Paper No. 3.49

P.M. Byrne
Professor, Dept. of Civil Engineering, University of B.C., Vancouver, B.C., Canada

J. McIntyre
Klohn-Crippen Consultants Ltd., Richmond, B.C., Canada

SYNOPSIS An incremental stress-strain model for granular soils based on fundamental soil mechanics principles is presented. The model captures the drained skeleton behaviour observed in laboratory tests under cyclic loading. The undrained behaviour is captured using the same skeleton stress-strain relation together with the volumetric constraint imposed by the porewater fluid. The model predicts cyclic simple shear response in close agreement with observed cyclic test data in terms of porewater pressure rise, cycles to trigger liquefaction, as well as the characteristic post-liquefaction response. Finally, the model is incorporated in a dynamic analyses procedure and applied to the field case history recorded at the Wildlife site. The recorded downhole time history was used as input and the predicted response compared with the field observation. In general, the agreement is good except for the porewater pressure response, which showed a more rapid rise than was observed.

INTRODUCTION

Cyclic shear loading causes a tendency for volumetric compaction of granular material, whether it be loose or dense. If the pores of the material are filled with a fluid that can either compress or escape during the loading, then an actual volumetric contraction will occur. If, on the other hand, the pores are filled with an essentially incompressible fluid, such as water, and if this fluid cannot escape during the period of shaking, then the tendency for volume change will transfer the normal load from the soil skeleton to the water, causing a rise in porewater pressure and a reduction in effective stress.

As the effective stress reduces, both the modulus and strength reduce leading to increased shear strains. If the effective stress drops to zero, the shear modulus will also be essentially zero and the soil will behave as a liquid - a state of transient liquefaction. This state only exists at the instant when the shear stress is zero. As the soil undergoes large shear strain at low confining stress, it will dilate causing the porewater pressure to drop and the effective stress to rise. This in turn causes the element to strain-harden and develop some stiffness and strength depending on its density. Loose sands may develop only a small amount of stiffness and strength, whereas dense sands will quickly develop a high strength and stiffness.

This paper presents examination of the response of a granular medium to cyclic load. The shear and volumetric strain responses of the dry or drained skeleton are first examined and a relatively simple incremental model that captures the laboratory data proposed.

The saturated undrained response to cyclic loading is captured using the same skeleton model as for the drained condition and applying the volumetric constraint that arises from the presence of the porewater fluid. The undrained model is validated by comparison with laboratory cyclic test data in terms of both porewater pressure rise and triggering of liquefaction as well as the post-triggering response.

Finally the model is used in the dynamic mode to predict the response at the Wildlife site in California where liquefaction occurred during an earthquake in 1987. Accelerations measured both above and below the liquefied layer, as well as porewater pressure measurement in the liquefied layer, allow a comparison between predicted and measured field response.

ANALYSIS PROCEDURE

The analysis of a soil-structure system subjected to earthquake loading is complex. The structure can be modelled as comprising a number of elements that prior to the earthquake loading, are generally under a range of static stresses (Fig. 1). Under earthquake loading each element will be subjected to a time history of normal and shear stresses (cyclic stresses) starting from a different static bias. In addition, these cyclic stresses themselves depend on the stress-strain response of the elements. As the stiffness of the element drops, due to rise in porewater pressure, the overall period of the structure will increase. This in turn may increase or decrease the structure response and element dynamic stresses, depending on the predominant period of the input motion.

A rational response analysis requires a solution in the time domain taking into account the stress-strain-porewater pressure response of each element. Therefore, the essence of the problem is the formulation of an element stress-strain and porewater pressure model that captures the observed laboratory element response up to and including triggering of liquefaction, as well as the post-triggering phase. Once the element behaviour is captured, it can be incorporated in a

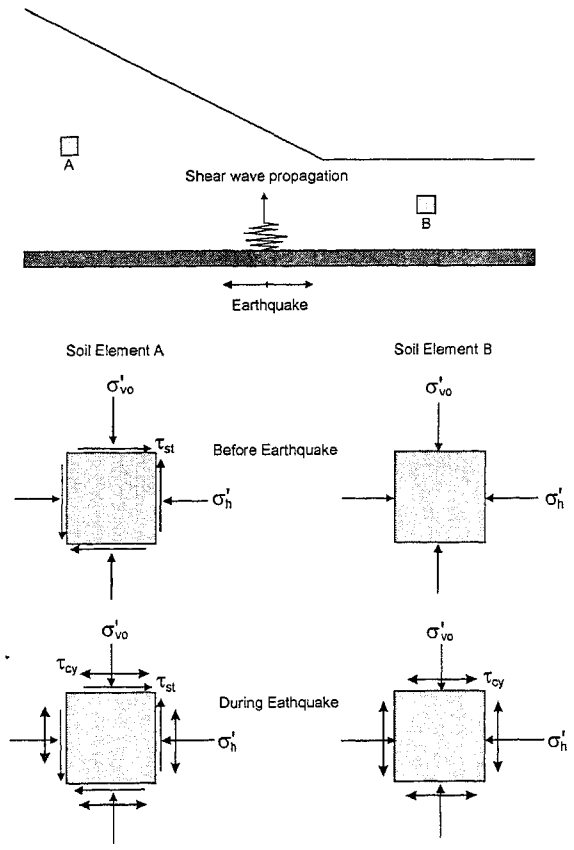

Fig. 1: Elements under static and seismic loading conditions.

finite element or finite difference code to predict the response of the soil-structure system to the specified time history of loading.

The purpose here is to present an incremental stress-strain model that captures the element or laboratory test response for both drained and undrained conditions and validate it by comparison with observed field behaviour. A key factor in the response of granular material to both monotonic and cyclic loading is the coupling that occurs between shear and volumetric strains, i.e., shear strains induce volumetric strains. It is this shear-volume coupling that induces the rise in porewater pressure when the porewater is prevented from leaving the skeleton by a drainage constraint.

SHEAR-VOLUME COUPLING

Empirical Approach

Shear strains induce volumetric strains in unbonded granular soil, and cyclic shear strains cause an accumulation of volumetric compaction strain with number of cycles (Fig. 2). The first shear-volume coupling model was presented by Martin-Finn-Seed (1975). This model was based on simple shear test data and would simulate earthquake loading under level ground conditions. The increment of volumetric strain per cycle of shear strain, γ, was expressed as follows:

$$(\Delta\varepsilon_v)_{cycle} = C_1(\gamma - C_2\varepsilon_v) + \frac{C_3\varepsilon_v^2}{\gamma + C_4\varepsilon_v} \quad (1)$$

in which

$(\Delta\varepsilon_v)_{cycle}$ = the increment of volumetric strain in percent per cycle of shear strain,

ε_v = the accumulated volumetric strain from previous cycles in percent,

γ = the amplitude of shear strain in percent for the cycle in question, and

C_1, C_2, C_3, C_4 = constants for the sand in question at the relative density under consideration.

This formulation as discussed by Byrne (1991) is unnecessarily complex and is not generally stable. He proposed that the data base presented by Martin et al. can be better modelled by

$$(\Delta\varepsilon_v)_{1/2\,cycle} = 0.5\,\gamma\,C_1\,EXP\left(\frac{-C_2\varepsilon_v}{\gamma}\right) \quad (2)$$

in which $(\Delta\varepsilon_v)_{1/2\,cycle}$ is the additional volumetric strain per half cycle of strain, γ, and ε_v is the accumulated strain. C_1 and C_2 are constants that depend on the relative density of the sand. This formulation was shown by Byrne to be in good agreement with available data.

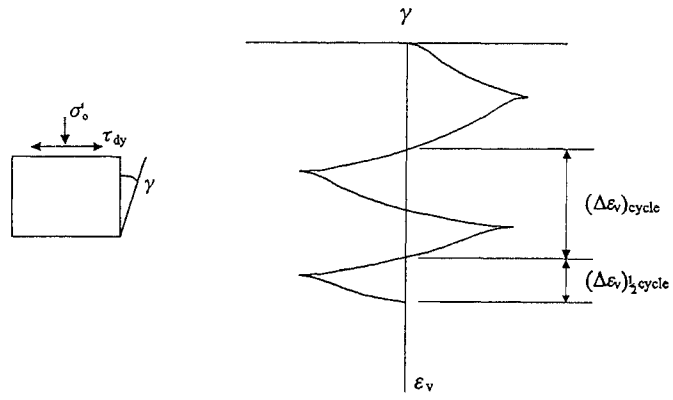

Fig. 2: Accumulation of volumetric strain due to cyclic shear strains.

Best fit values of C_1 as a function of relative density, D_r, or normalized standard penetration value, $(N_1)_{60}$ are shown in Table 1.

Table 1. C_1 in Terms of D_r and $(N_1)_{60}$

$(N_1)_{60}$	D_r	C_1
5	34	1.00
10	47	0.50
20	67	0.20
30	82	0.12
40	95	0.06

The constant C_2 is related to C_1 as follows:

$$C_2 = 0.4/C_1 \quad (3)$$

So that only one constant is needed to specify the density effect.

While this formulation can be used in a loose coupled analysis, it is not appropriate for a coupled incremental analysis. For such a formulation the increment of volumetric strain, $d\varepsilon_v$, as a function of the increment of shear strain, $d\gamma$, is required for each time step rather than every 1/2 cycle. The simplest incremental formulation based on Eq. (2) is obtained by assuming that the volumetric strain develops linearly with shear strain during any half-cycle, from which:

$$d\varepsilon_v = 0.25\, d\gamma\, C_1\, EXP\left(\frac{-C_2\varepsilon_v}{\gamma}\right) = d\gamma \cdot D_t \quad (4)$$

in which γ is the largest strain in the current 1/2 cycle. The terms associated with $d\gamma$ can be lumped into a single shear-volume coupling term, D_t.

This is a satisfactory approach when the shear strain sequence is known a priori and gives essentially the same result as Eq. (2). However, for the earthquake problem, the strain sequence is not known ahead of time. One solution is to assume γ to be the largest strain in the current or previous cycle, whichever is larger.

This empirical approach is satisfactory for simple shear conditions in the absence of a static bias. For a more general initial stress state, and for conditions after triggering of liquefaction, a more fundamental approach is desirable and this has been described by Byrne and McIntyre, 1994. Their stress-strain characterization of soil is shown in Fig. 3.

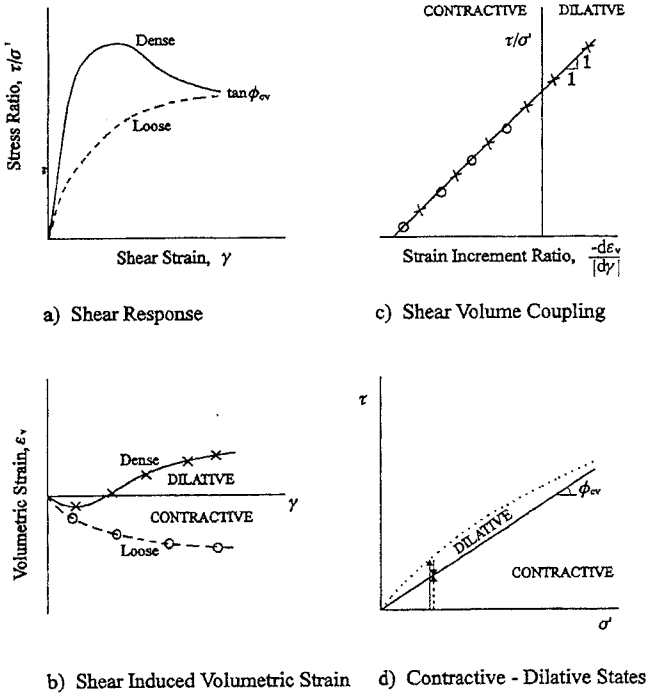

Fig. 3: Stress-strain and volume change response of the granular skeleton to monotonic simple shear loading.

Their more fundamental shear volume coupling equation is given by

$$d\varepsilon_v^p = d\gamma^p\left(\mathrm{Tan}\phi_{cv} - \tau/\sigma'\right) = d\gamma^p \cdot D_t \quad (5)$$

where τ/σ' is the stress ratio and ϕ_{cv} is the constant volume friction angle of the soil. The superscript denotes plastic strains.

Shear-volume coupling effects under strain controlled conditions can be computed from the empirical Eq. (4) which captures the laboratory data. They can also be computed from the more fundamental Eq. (5). For load controlled conditions which arise in earthquake and other cyclic load situations it is first necessary to compute the increment of shear strain from the shear stress-strain law and this is next addressed.

SHEAR STRESS-STRAIN LAW

The simplest shear stress-strain law that is in reasonable accord with laboratory data is the Hyperbolic Formulation (Duncan and Chang, 1970). The tangent stiffness G_t at any stress state is defined as:

$$G_t = \frac{d\tau}{d\gamma} = G_{max}\left(1-\frac{\tau}{\tau_f}R_f\right)^2 \quad (6)$$

in which

G_{max} = the maximum shear modulus that occurs at zero shear strain.

τ = the shear stress,

τ_f = the failure shear stress,

R_f = the failure ratio τ_f/τ_{ult} in which τ_{ult} is the ultimate strength from the best fit hyperbola

The parameter R_f is used to modify the hyperbola to fit the laboratory data. For most sands, R_f lies between 0.5 and 0.9 for monotonic loading.

The shear stress-strain relation under cyclic loading can also be modelled as a hyperbola and the tangent stiffness at any stress level expressed by

$$G_t = G_{max}\left(1-\frac{\tau^*}{\tau^*_f}R_f\right)^2 \quad (7)$$

where

G_{max} = the shear modulus immediately upon unloading.

τ^* = $(\tau_A +/- \tau)$

τ^*_f = $(\tau_A + \tau_f)$, and

τ_A = the shear stress at the reversal point as shown in Fig. 4.

The increment of shear strain, $d\gamma$, for an applied increment of shear stress, $d\tau$, is, therefore,

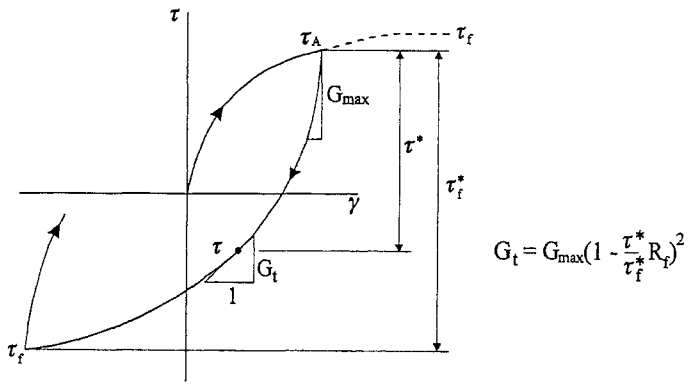

Fig. 4: Shear Stress-Strain Model for Unload-Reload.

$$d\gamma = \frac{1}{G_t} d\tau \tag{8}$$

A more general formulation for sand is discussed in detail by Byrne and McIntyre 1994.

SKELETON STRESS-STRAIN RELATIONS

The response of the skeleton to simple shear loading is obtained as follows:

- The increment of shear strain $d\gamma$ is computed from Eq. (8),
- The increment of volumetric strain $d\varepsilon_v$ from Eq. (4) or (5),
- The increment of elastic volumetric strain, $d\varepsilon_v^e$ from

$$d\varepsilon_v^e = \frac{d\sigma'}{M} \tag{9}$$

where M is the constrained modulus.

For a drained simple shear test, the stress increment $d\tau$ can be selected ($d\sigma$ =0), and the strain increments computed as described above. The stress-strain and volumetric strain response is then obtained by summation of the increments. In this case $d\varepsilon_v^e$ = 0 and the total and plastic volumetric strains are equal.

UNDRAINED RESPONSE

If drainage of porewater fluid is prevented from occurring during the application of a load increment, a volumetric constraint is imposed on the skeleton. The response of the skeleton is predicted here using the same skeleton model described in the previous section but taking into account the volumetric constraint of the porewater fluid.

If the porewater fluid and solids are assumed incompressible, the overall volumetric strain will be zero. However, grain slip will still occur within the skeleton causing both plastic shear and plastic volumetric strains such that:

$$d\varepsilon_v = d\varepsilon_v^e + d\varepsilon_v^p = 0 \tag{10}$$

Now $d\varepsilon_v^e = d\sigma'/M$, hence from Eq. (10),

$$d\sigma' = -M d\varepsilon_v^e = -M\ D_t\ d\gamma^p \tag{11}$$

Since $d\sigma' = d\sigma - du$, and for conventional simple shear tests or 1-D field conditions $d\sigma = 0$, the rise in porewater pressure $du = -d\sigma'$, therefore

$$du = M d\varepsilon_v^e = M\ D_t\ d\gamma^p \tag{12}$$

The increment of shear strain for undrained conditions $d\gamma$ is obtained from:

$$d\gamma = d\tau/G_t \tag{13}$$

where

$$G_t = G_{max}\left(1 - \frac{\tau}{s_u} R_f\right)^2 \tag{14}$$

and

$$G_{max} = k_g\ Pa \left[\frac{\sigma_v - u}{Pa}\right]^{1/2} \tag{16}$$

and s_u = the residual undrained strength of the soil.

The analysis procedure involves computing $d\gamma$ from Eq. 13 and the pore pressure increment from Eq. 12. The excess pore pressure u is obtained at each step by summing the pore pressure increment from Eq. 12.

MODEL CALIBRATION

The key input parameters to the model are:

1) The maximum shear modulus, G_{max} described by k_g.
2) The undrained strength, S_u.
3) The constant volume friction angle ϕ_{cv}.
4) The failure ratio, R_f.
5) The rebound constrained modulus, M.
6) The relative density of the soil.

These have been related to the normalized penetration resistance value $(N_1)_{60}$ as described in detail by Byrne (1991).

The model has been calibrated against the Seed et al. (1984) liquefaction chart, so that, for example, a simple shear element under a vertical effective stress of 1 T/ft^2, and subject to a cyclic stress ratio of 0.11 will liquefy in about 15 cycles in agreement with the chart.

The predicted cyclic shear stress-strain and effective stress path response for a cyclic load controlled test are shown in Fig. 5. It may be

seen (Fig. 5a) that the stress-strain response remains stiff for a number of cycles until the porewater pressure rise causes the effective stress state to reach the ϕ_{cv} line (point A, Fig. 5b). The material then deforms with a low modulus and large strain as it moves up the ϕ_{cv} line to point B (dilative). Upon unloading from B, the soil is initially very stiff but is also very contractive so that it generates a large porewater pressure rise that may drive the effective stress point to zero at point C, when $\tau = 0$. The material is essentially a liquid at this point ($G_t \approx 0$) and large strains occur. With further increase in strain, the material eventually dilates causing a drop in porewater pressure and the stress point moves up the ϕ_{cv} line, stiffening as it goes. Upon unloading from D, the process is repeated leading to large cyclic strains commonly referred to as cyclic mobility or cyclic liquefaction.

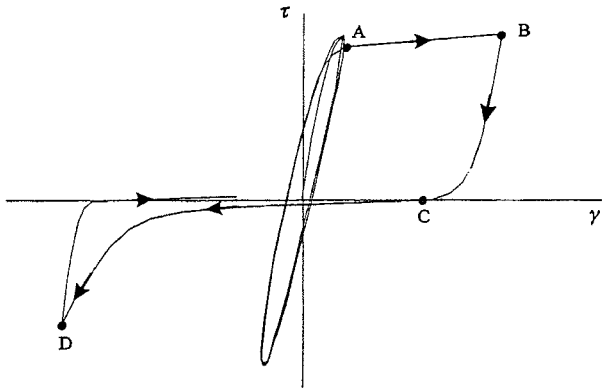

a) Shear stress-strain response

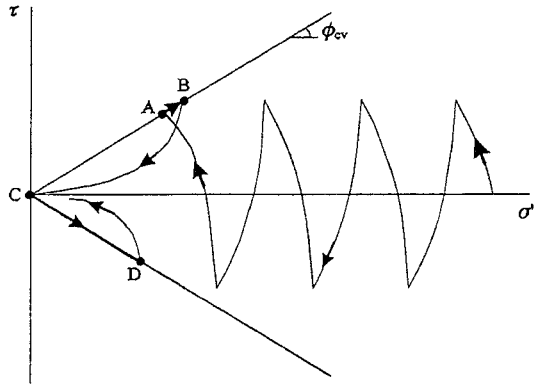

b) Effective stress path response

Fig. 5: Predicted cyclic shear stress-strain and effective stress path response for a cyclic load controlled test.

This predicted behaviour is in agreement with observed laboratory cyclic simple shear data. In fact, the model has been calibrated to capture the laboratory data.

Having captured the element behaviour, the next check in the validation procedure is to incorporate the element response in a dynamic analysis and predict and compare with a field event, and this is described in the section which follows.

FIELD VERIFICATION

Background

The model was used to predict the dynamic response of the Wildlife site - an instrumented site where liquefaction occurred during an 1987 earthquake. The Wildlife site is located in southern California in the seismically active Imperial Valley. The site was instrumented in 1982 by the U.S. Geological Survey using accelerometers and piezometers in an effort to record ground motions and porewater pressures during earthquakes.

Site Description

The Wildlife site is located in the floodplain of the Alamo River approximately 36 km north of El Centro. Although the site is on level ground, it is located in close proximity (about 20m) to the river's western bank. In-situ and laboratory investigations (Bennett et al. 1984) have shown that the site stratigraphy consists of a surficial silt layer approximately 2.5 m thick underlain by a 4.3 m thick layer of loose silty-sand, underlain by a stiff to very stiff clay. The groundwater table fluctuates within the surficial silt layer at a depth of about 2.0 m.

Instrumentation

The liquefaction array at the Wildlife site consists of two 3-component accelerometers and six electric piezometers. One accelerometer was mounted at the surface on a concrete slab supporting an instrument shed. The second accelerometer was installed in a cased hole beneath the liquefiable layer at a depth of 7.5 m. Five of the six piezometers were installed within the liquefiable sand layer. Details about the instrumentation and the installation procedure are given by Youd and Wieczorek (1984).

Recorded Site Response

In November, 1987 the Wildlife site was shaken by two earthquakes - the Elmore Ranch earthquake and the Superstition Hills earthquake. Both events triggered the instrumentation at the site; however, only the Superstition Hills earthquake (M = 6.6) generated dynamic porewater pressures. Subsequent site investigations showed evidence of liquefaction in the form of sand boils and small ground fissures (Zeghal and Elgamal, in review).

Fig. 6 shows the measured acceleration time histories for the North-South component of the Superstition Hills quake. Fig. 6(a) shows the surface time history while the downhole time history is shown in Fig. 6(b). Surface and downhole displacement time histories were obtained by integration of the acceleration time histories, and are shown in Fig. 7(a) and Fig. 7(b) respectively.

Relative displacements between the surface and the stiff base are of prime interest and these were obtained by subtracting the surface and downhole displacement time histories at each time increment. The resulting relative displacement time history is shown in Fig. 7(c). Note that the relative displacements were essentially zero for about the first fourteen seconds of shaking despite the fact that significant displacements were measured both at the surface and downhole. This indicates that up until fourteen seconds, the soil units above and below the liquefiable sand

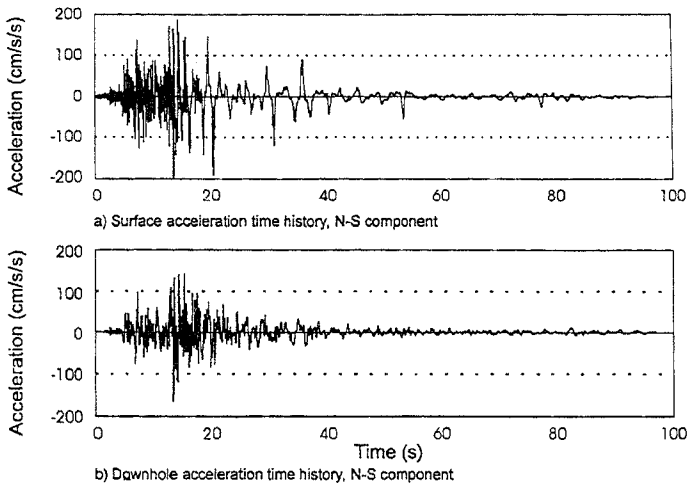

Fig. 6: Acceleration time histories - Wildlife Site, 1987 Superstition Hills earthquake

layer essentially moved together. After fourteen seconds, significant relative displacements occurred, indicating the uncoupling of the soil units above and below the sand layer.

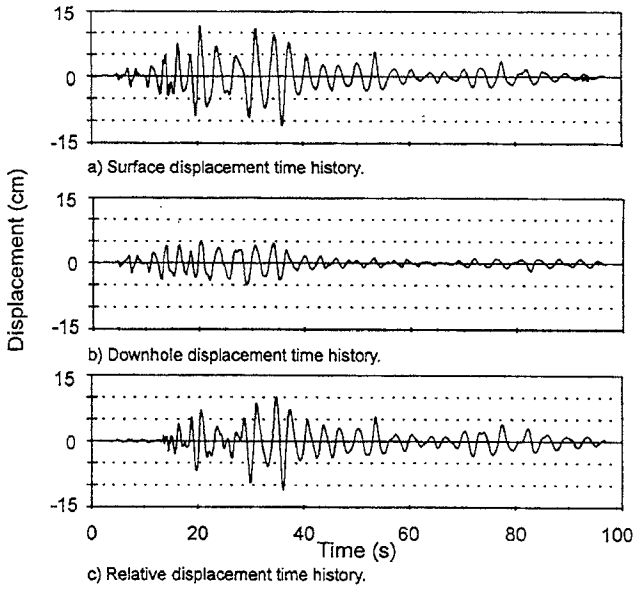

Fig. 7: Displacement time histories - Wildlife Site, 1987 Superstition Hills earthquake.

The recorded time history of surface acceleration versus relative displacement is shown in Fig. 8. This plot is similar to a shear stress versus shear strain plot, as shear stress would simply be the surface acceleration multiplied by the soil mass, and the strains would be the relative displacements divided by the thickness of the liquefied layer. Since neither the soil mass nor the thickness of the liquefied layer are known with certainty, presenting the data in this form introduces less error.

By isolating brief segments of the data from Fig. 8, it is possible to see how the soil modulus

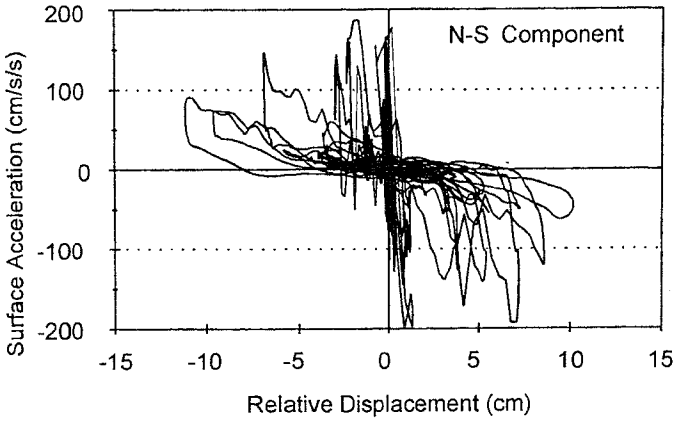

Fig. 8: Surface acceleration vs. relative displacement; Wildlife Site, 1987 Superstition Hills earthquake.

changes with cycles. Fig. 9 shows four discrete cycles at different times during the earthquake. For about the first 14 seconds of shaking, the soil is stiff as shown in Fig. 9(a) and there has been little degradation of modulus. At about 16 seconds (Fig. 9b) significant degradation of modulus has occurred. At 35 seconds (Fig. 9c), further degradation of modulus has occurred with a flat zero modulus zone followed by strain-hardening and an abrupt increase in modulus upon unloading.

The behaviour shown in Fig. 9(c) is typical of a cyclic laboratory simple shear response after liquefaction has been triggered, and is caused by repeated dilatant and contractant response as the stress point cycles through the zero effective stress state as discussed previously. This same behaviour is seen in Fig. 9(d), except the base accelerations are considerably smaller at this stage of the earthquake.

The approximate 500 fold reduction in soil stiffness that occurs after roughly 18 seconds of shaking is a clear indication to the authors that effective stresses have reduced to near zero and liquefaction has been triggered, at least in some zones of the soil profile.

Analysis Procedure

The dynamic analysis of the site was carried using a single-degree-of-freedom lumped mass and spring model. The lumped mass involved both the mass of the 2.5 m surficial crust and the 1/2 thickness of the 4.3 m liquefiable layer. The spring was nonlinear and represented the stiffness of the liquefiable layer by incorporating the stress-strain model discussed earlier. The downhole time history of acceleration was applied as base input motion and the response of the system obtained by step-by-step integration in the time domain. The computed response in terms of surface accelerations, relative displacements, and porewater pressures are compared in the next section.

Results

The predicted and observed surface accelerations are shown in Fig. 10(a) where it may be seen that the general form of the predicted response is in

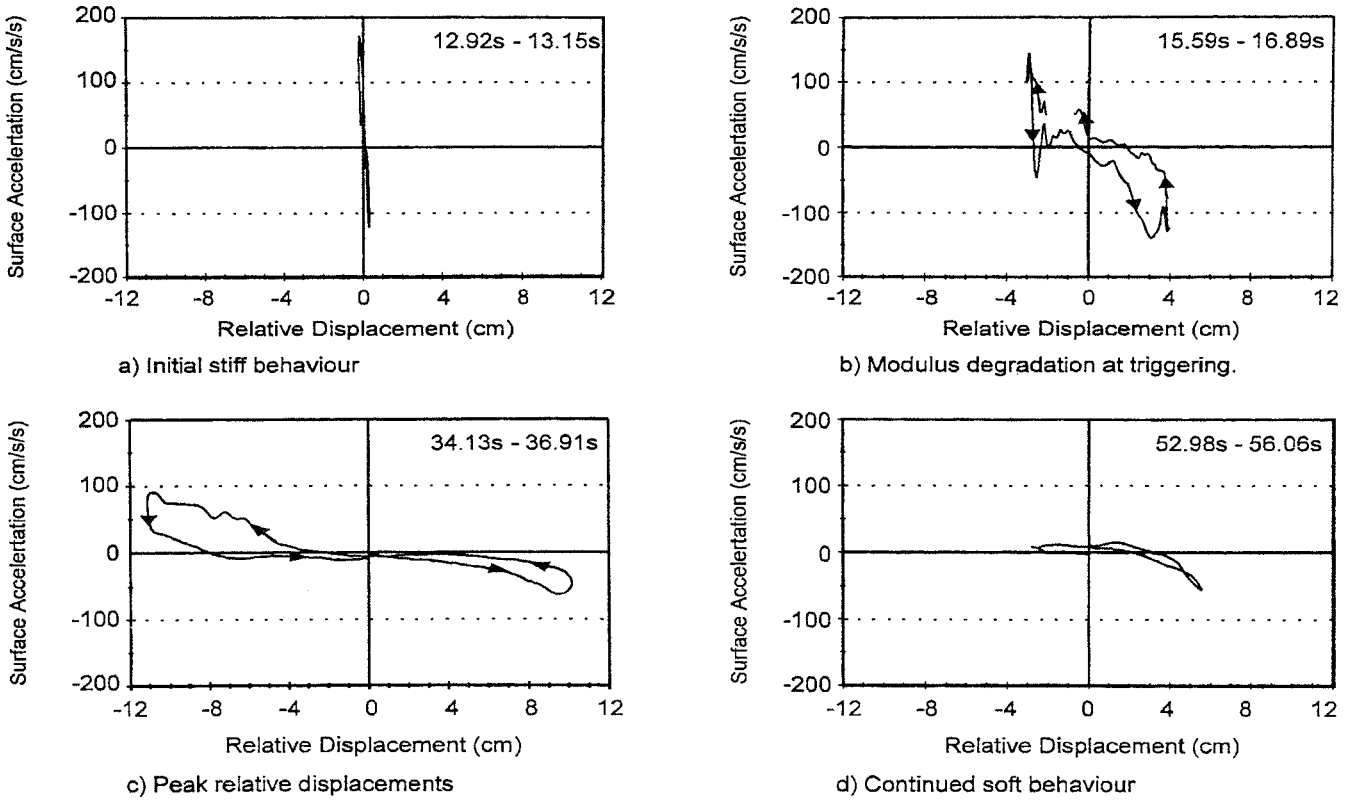

Fig. 9: Change in soil stiffness during selected cycles - Wildlife Site, 1987 Superstition Hills earthquake.

reasonable accord with the observation. The predicted and observed relative displacements are shown in Fig. 10(b), where it may be seen that up to about 17 seconds both computed and measured relative displacements are very small. After 17 seconds relatively large displacement oscillations are predicted. It may be seen that both the pattern and magnitude of predicted and observed displacements are in reasonable accord.

The predicted surface acceleration versus relative displacement pattern is shown in Fig. 11(a). Prior to about 17 seconds the loops are very steep. At this point, liquefaction is triggered causing very flat loops that are in general accord with the observed pattern shown in Fig. 8. However, Fig. 8 shows a less abrupt degradation of modulus than the model prediction. This may be the result of a gradual spreading of the zone of liquefaction with time as compared to the assumption made in the analysis that the whole zone liquefied at one time.

The predicted effective stress path is shown in Fig. 11(b). It may be seen that the effective stress point gradually worked its way back from an initial state of σ'_{vo} = 66 kPa and τ_{st} = 0. This occurred as the shaking caused cyclic shear stress pulses and associated porewater pressure rise. It may be seen that the stress point reached the phase transformation or ϕ'_{cv} line a few times before the developed strain was sufficient to trigger a large porewater pressure rise and drive the stress point to the zero effective stress state upon unloading. Once this state was reached, subsequent butterfly loops up the σ'_{cv} line and down within the ϕ'_{cv} line, are predicted to occur with accompanying porewater pressure oscillations.

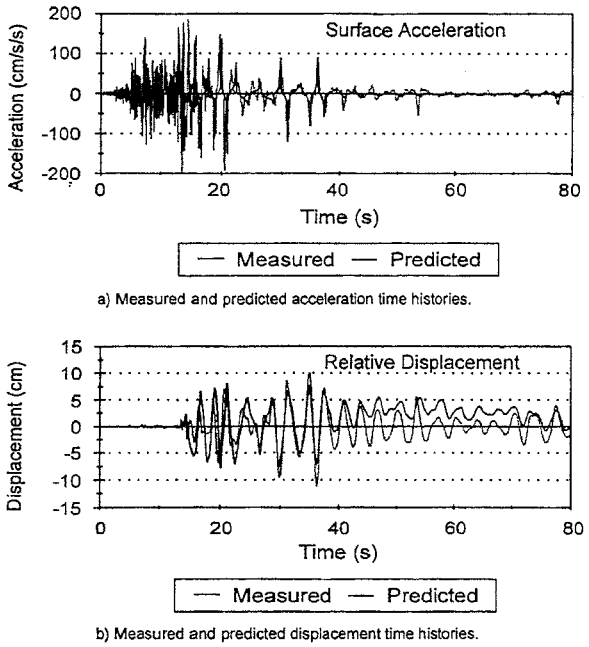

Fig. 10: Comparison of measured and predicted time histories - Wildlife Site, 1987 Superstition Hills earthquake.

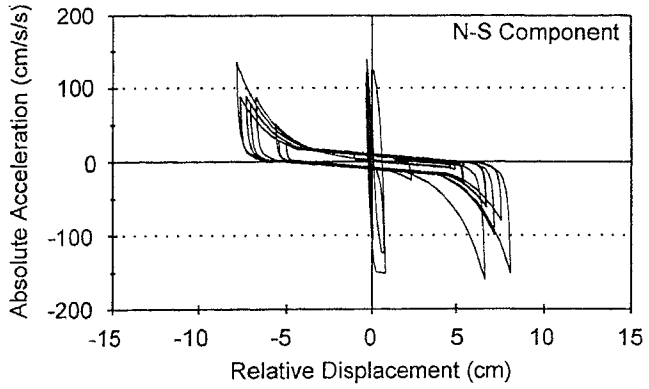

a) Acceleration versus relative displacement.

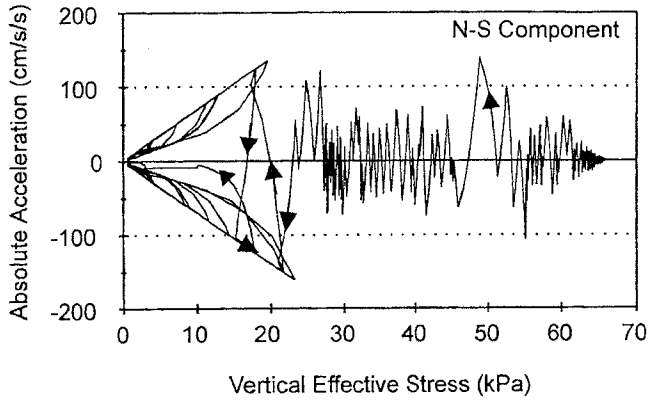

b) Acceleration versus vertical effective stress.

Fig. 11: Predicted dynamic response of Wildlife Site for 1987 Superstition Hills earthquake.

The predicted and observed porewater pressure ratios are shown in Fig. 12. It may be seen that the predicted porewater pressure rise is much faster than the measured rise and shows significant oscillations due to dilation after liquefaction has been triggered. The measured porewater pressure response does show significant pulses after about 30 seconds when about 80% porewater pressure rise occurs. These would

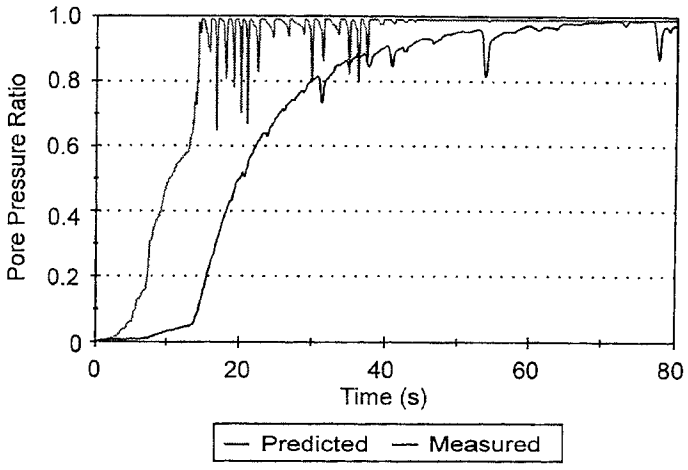

Fig. 12: Comparison between measured and predicted pore pressure ratios - Wildlife Site, 1987 Superstition Hills earthquake.

appear to correspond with dilation pulses after liquefaction has been triggered. Numerous explanations have been proposed to explain the apparent lag in porewater pressure rise (Thilakaratne and Vucetic, 1989; Zeghal and Elgamal, in review).

The measured relative displacements shown in Fig. 7(c) indicate that liquefaction was triggered at some depth within the liquefiable layer at about 17 seconds. If piezometer #5 (Fig. 12) is reading correctly, it would suggest that liquefaction did not occur at this location until about 50 secs.

SUMMARY

The characteristic shear stress-strain and volumetric response of the granular skeleton is captured using an incremental stress-strain law. The shear behaviour in both loading and unloading is modelled by modified hyperbolas, and shear-volume coupling is included. The concept of contraction below the phase transformation or ϕ_{cv} line, and dilation above after triggering is incorporated.

The model is first calibrated in the drained mode by comparison with available laboratory data on volumetric accumulation with cycles of shear strain. Undrained response is predicted by imposing a volumetric constraint on the granular skeleton. The model captures the undrained laboratory test data in terms of the degradation of the shear stress-strain response with porewater pressure rise during cyclic loading. It also captures the effective stress path followed as the stress state moves to the phase transformation or ϕ_{cv} line to trigger liquefaction, as well as the complex butterfly loops observed after triggering.

Finally, the model is incorporated in a dynamic analysis procedure and applied to the field case history recorded at the Wildlife site in California in 1987. The recorded downhole time history of acceleration was used as input to the dynamic model and the predicted response, in terms of surface acceleration, relative displacement, and porewater pressure compared with the measurements.

The predicted and observed surface acceleration are in reasonable agreement in terms of both the amplitude and characteristic frequency of response. The relative displacements are also in reasonable agreement with observations. In particular, the relative displacement pattern after 17 seconds, at which time we believe liquefaction was triggered, is in good agreement.

The predicted acceleration versus relative displacement (stress versus strain) curves are in very good agreement and indicate that prior to t = 17 seconds the stress-strain response is very stiff, whereas after this time a major reduction in stiffness by a factor of about 500 occurs. This indicates that liquefaction and essentially 100% porewater pressure rise was triggered at least in some zones at about t = 17 seconds.

The predicted porewater pressures are not in good agreement with the measurements. The predicted porewater pressure rise is much faster than the measured values. The slower measured response is thought to be due to either compliance in the measuring system or to the possibility that

liquefaction did not occur simultaneously at all points in the liquefied layer.

ACKNOWLEDGEMENT

The authors acknowledge the financial support of NSERC Canada in this work. They are grateful to Mrs. K. Lamb for her typing and presentation of the paper.

REFERENCES

Been, K. and Jefferies, M.G. (1985). "A State Parameter for Sands," Geotechnique, Vol. 35, No. 2, pp. 99- 112.

Bennett, M.J., McLaughlin, P.V., Sarmiento, J. and Youd, T.L. (1984). "Geotechnical Investigation of Liquefaction Sites, Imperial Valley, California," US Geological Survey Open File Report 84-242, pp. 1-103.

Byrne, P.M. (1991). "A Cyclic Shear Volume - Coupling and Porewater Pressure Model for Sand," Second International Conference on Recent Advances in Geotechnical Earthquake Engineering and Soil Dynamics, St. Louis, Missouri, Report 1.24, Vol. 1, March, pp. 47-56.

Duncan, J.M. and Chang, Y.Y. (1970). "Nonlinear Analysis of Stress and Strain in Soils," Journal of the Soil Mechanics and Foundations Division, ASCE, Vol. 96, No. SM5, September.

Holzer, T.L., Bennett, M.J. and Youd, T.L. (1989). "Lateral Spreading Field Experiments by the US Geological Survey," Proceedings, 2nd US-Japan Workshop on Liquefaction, Large Ground Deformation and Their Effects on Lifelines, Buffalo, New York, pp. 82-101.

Lee, C.-J. (1991). "Deformation of Sand Under Cyclic Simple Shear Loading," Second International Conference on Recent Advances in Geotechnical Earthquake Engineering and Soil Dynamics, St. Louis, Missouri, Report 1.12, Vol. 1, March, pp. 33-36.

Martin, G.R., Finn, W.D. Liam and Seed, H.B. (1975). "Fundamentals of Liquefaction Under Cyclic Loading," Journal of the Geotechnical Engineering Division, ASCE, May, Vol. 101, No. GT5.

Matsuoka, H. and Nakai, T. (1977). "Stress-Strain Relationship of Soil Based on SMP," Proc., Specialty Session 9, 9th ICSMFE, pp. 153-162.

Schofield, A. and Wroth, P. (1968). "Critical State Soil Mechanics," published by McGraw-Hill, pp. 124-127.

Seed, H.B., Tokimatsu, K., Harder, L.F. and Chung, R. (1985). "Influence of SPT Procedures in Soil Liquefaction Resistance Evaluations," Journal of Geotechnical Engineering, ASCE, Vol. 111, No. 12.

Taylor, D.W. (1948). "Fundamental of Soil Mechanics," published by John Wiley and Sons, pp. 346-347.

Thilakaratne, V. and Vucetic, M. (1989). "Liquefaction at the Wildlife Site - Effect on Soil Stiffness on Seismic Response, Proceedings, 4th International Conference on Soil Dynamics and Earthquake Engineering, Mexico City, pp. 37-52.

Tokimatsu, K. and Seed, H.B. (1987). "Evaluation of Settlements in Sands Due to Earthquake Shaking," Journal of Geotechnical Engineering, ASCE, 1987, Vol. 113, No. 8, pp. 861-878.

Youd, T.L., Holzer, T.L. and Bennett, M.J. (1989). "Liquefaction Lessons Learned from Imperial Valley, California," Earthquake Geotechnical Engineering, Proceedings of Discussion Session, 12th International Conference on Soil Mechanic and Foundation ngineering, Rio de Janeiro, Brazil, 47-54.

Youd, T.L.and Wieczorek, G.F. (1994). "Liquefaction During the 1987 and Previous Earthquakes Near Westmorland, California," US Geological Survey Open-File Report 84-680.

Zeghal, M. and Elgamal, A.W. (in review). "Analysis of Wildlife Site Using Earthquake Records," Journal of Geotechnical Engineering, ASCE, submitted to ASCE Journal of Geotechnical Engineering.